# Quantum Chemical Study on Excited States and Electronic Coupling Matrix Element in a Catechol−Bridge−Dicyanoethylene System

**Rong-Xing He, Xiao-Hui Duan, and Xiang-Yuan Li***

*College of Chemical Engineering, Sichuan University, Chengdu 610065, People's Republic of China*

*Received: September 5, 2004; In Final Form: March 8, 2005*

The excited states of a donor−bridge−acceptor (DBA) model system have been investigated using time-dependent density-functional theory (TD-DFT) in vacuo and in solution. It is found that the MPW1PW91 functional always gives higher excitation energies than those with a B3LYP functional. Results from both TD-B3LYP and TD-MPW1PW91 are found consistent with the experimental observations. The two most intense absorptions of the DBA system, one resulting from the local excitation of catechol moiety and the other from that of dicyanoethylene, possess the $\pi\pi^*$ transition feature. It seems that the solvent polarity does not remarkably influence the positions of absorption peaks. The spectroscopic properties of isolated donor, acceptor, and bridge and the donor−bridge compound have been investigated at the TD-B3LYP/6-31+G* and TD-MPW1PW91/6-31+G* levels. Results indicate that the donor and the acceptor are weakly coupled with the bridge. Therefore, it is more likely that the electron transfer takes place through a superexchange mechanism. In addition, we calculate the electronic coupling matrix elements according to the generalized Mulliken−Hush theory, and the detailed analyses also predict that the strong absorptions are due to the local excitation of the DBA system.

## 1. Introduction

Electron transfer (ET) between chemical species and subunits of a single compound is one of the most fundamental processes in many biological processes[1,2] and in material science.[3,4] The photoinduced ET reaction recently attracted much attention triggered by its possible applications in the fabrication of electrooptical switches, chemical sensors, fluorescence probes, and molecular switches.[5−14] An ideal device requires a unique molecular bridge between the donor and the acceptor chromophores, so that the transfer of the electron can be regulated in a controlled manner.[15−16] Recently, Chiou and Chow synthesized and applied a new rod-shaped molecule, heptacyclo-[6.6.0.0$^{2,6}$.0$^{3,13}$.0$^{4,11}$.0$^{5,9}$.0$^{10,14}$]tetradecane (HCTD), as a bridge (B) between a donor (D) and an acceptor (A).[17−19] They expected that the DBA system (see Chart 1) could serve as a heuristic model in the processes of biological ET and of photosynthesis. By means of the time-resolved absorption spectroscopy, Chiou et al. investigated the feature of absorption spectra and the solvent effect.

By means of time-dependent density-functional theory (TD-DFT),[20−25] the authors have investigated the photoinduced electron transfer of the donor/acceptor pair via the rigid and linear bridge HCTD[19] in this work. Our main goal here is to characterize the lowest energy spectroscopic transitions of the DBA in vacuo and in solvents. In the experimental aspect, Chiou et al. concluded that the 280 nm maximum absorption of DBA is from the local $\pi\pi^*$ transition of the catechol group, but the strong band at 230 nm is from the local excitation (LE) on the dicyanoethlene moiety. Moreover, in solvents, the concentration of the excited charge transfer species is negligibly small. In addition, according to the experimental observations, the absorption maximum of DBA is independent of the solvent polarity.

**CHART 1**

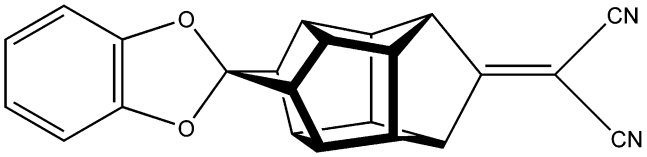


To the best of our knowledge, no ab initio results about the absorption spectra and the solvent effects of this DBA system have been published.

Theoretical investigations may provide insight into the possible pathways for ET processes and highlight the crucial role played by the electronic coupling between D and A, because the electronic coupling governs the distance dependence of the ET rates.[26] In long-range intramolecular ET, two mechanisms are often used to describe the ET reactions, one is the so-called superexchange and the other is the bridge-mediated mechanism. When D and A are weakly coupled with B, the electron transfers directly from D to A, via a tunneling process, or in other words, via superexchange. The rate constant of ET exhibits an exponential decay as a function of the distance, *d*, between D and A, i.e.,

$$k_{RP} \approx \exp(-\beta d) \qquad (1)$$

In eq 1, $\beta$ varies typically from 0.2 to 1.4 Å$^{-1}$,[27−31] depending on the system. In the bridge-mediated mechanism, the coupling is strong, and the ET occurs via the "bridge", that is, the electron is at first transferred from the excited donor (denoted as D*) to the adjacent bridge, and then from the bridge to the acceptor. In the present paper, we attempt to make clear the possible pathways of ET in this DBA system.

This paper is organized as follows. Computational details are briefly described in the next section. In section 3.1, the in vacuo

* Correspondence author. E-mail: xyli@scu.edu.cn.

10.1021/jp045999h CCC: $30.25 
Published on Web 04/20/2005

absorptions are investigated with B3LYP and MPW1PW91 functionals in combination with the 6-31+G* basis set, and the comparison with experimental results has been made. In section 3.2, in vacuo absorptions of isolated species and the donor−bridge system (DB) are calculated. Discussions on the mechanism of ET have been made. In section 3.3, the absorption spectra in solvents are studied. Then, the electronic coupling matrix element is estimated in section 3.4. Our conclusions are finally given in section 4.

## 2. Methodology

According to Fermi's golden rule, the ET rate constant $k_{et}$ is proportional to the square of the electron coupling matrix element $H_{ij}$, i.e.,[32−34]

$$k_{et} = \frac{2\pi}{\hbar} H_{ij}^2 (\mathrm{FCWD}) \tag{2}$$

where $\hbar = h/2\pi$, with $h$ being Planck's constant. The electronic coupling matrix element between the initial and final diabatic states $\Psi_i$ and $\Psi_j$ is defined as

$$H_{ij} = \langle \Psi_i | \mathrm{H} | \Psi_j \rangle \tag{3}$$

FCWD in eq 1 is a density-of-state weighted Franck−Condon factor taking into account the density of vibrational levels and the Franck−Condon overlap. This overlap incorporates the vibrational modes of the molecule, $\{\omega_i\}$, and those of the solvents, $\{\omega_s\}$.[35] If the condition of $h\omega_i \gg k_B T$ (here $k_B$ denotes the Boltzmann's constant) is satisfied, the vibrational modes of the molecule can be treated quantum mechanically, while a classical description can be taken for the solvent vibrational modes, since usually $h\omega_s \ll k_B T$. In such cases, the Franck−Condon factor can be written as[36]

$$\mathrm{FCWD} = \left(\frac{1}{4\pi\lambda_s k_B T}\right)^{1/2} \sum_v \mathrm{e}^{-S} \frac{S^v}{v!} \exp\left[-\frac{(\Delta G^0 + \lambda_s + v\hbar\langle\omega_i\rangle)^2}{4\lambda_s k_B T}\right] \tag{4}$$

where $\lambda_s$ describes the solvent reorganization energy, $\Delta G^0$ the variation of the Gibbs free energy change of the reaction, and $S$ the Huang−Rhys factor, i.e.,

$$S = \frac{\lambda_i}{\hbar\langle\omega_i\rangle}, \tag{5}$$

where $h\langle\omega_i\rangle$ is the effective mode vibrational energy, and $\lambda_i$ is the inner reorganization energy corresponding to the energy required to accommodate the nuclear rearrangements occurring upon charge transfer (CT) when going from the equilibrium geometry of the initial state to that of the final state.

To estimate the ET rate constant, $k_{et}$, and to study further the character of absorption spectra, the generalized Mulliken−Hush (GMH) theory for the nonperturbative calculation of $H_{ij}$ of ET is employed. Cave and Newton[37] developed the GMH formalism and expressed $H_{ij}$ as

$$H_{ij} = \frac{m_{ij}\Delta E_{ij}}{\sqrt{(\Delta\mu_{ij})^2 + 4(m_{ij})^2}}, \tag{6}$$

where $\Delta E_{ij}$ is the energy gap between the initial adiabatic state and the final one, $\Delta\mu_{ij}$ is the dipole moment difference between state $i$ and state $j$, and $m_{ij}$ is the transition dipole moment connecting the two states.

Prior to calculating excited states, the ground-state geometry optimization of the DBA system is performed in vacuo, at the B3LYP/6-31G* and MPW1PW91/6-31G* levels. Vertical transitions are investigated here, and the calculated excitation energies can be identified as band maxima in the experimental spectra.

Transition energies and oscillator strengths are calculated by using the TDDFT method implemented in the Gaussian 03 program.[38] TDDFT is now a well-established method to give reliable excitation energies for low-lying states.[20,21,23,39,40] In this work, the B3LYP and MPW1PW91 exchange-correlation functionals combined with 6-31G*, cc-pVDZ, 6-31+G*, and 6-31++G(d,p) basis sets are chosen for our purpose in solvents. The accuracy of the two functionals (B3LYP and MPW1PW91) for various compounds was discussed in refs 41−44.

It is essential to calculate the dipole moment according to eq 6. The dipole moment could be calculated by using the Hellmann−Feynman theorem, as the analytic derivative of the excited-state energy with respect to an applied electric field. More exact calculations are not available in the Gaussian program at present. Therefore, in the present paper, the dipole moments of excited states are estimated by using a finite field strategy (the field vector is ±0.001 au). Although the Runge−Gross theorem[45] establishing the validity of the TDDFT approach was only proven for potentials that decay to zero at infinity, this approach should be adequate for valence-like states because any integrals over the potential are finite due to the use of a truncated Gaussian basis set.

It is well-known that solvent has great influence on the electronic spectra owing to the interaction between the solute and the solvents. In this work, the nonequilibrium solvation energies in vertical transition processes are calculated by using the polarizable continuum model (PCM) to all calculations.[46−50]

## 3. Results and Discussions

**3.1. Gas-Phase Absorption of DBA.** The geometry of DBA is optimized at the B3LYP/6-31G* and MPW1PW91/6-31G* levels in vacuo. There is a slight difference in the structures of DBA optimized with B3LYP and MPW1PW91 functionals. The dipole moment of DBA at ground state is 6.51 D by B3LYP and 6.59 D by MPW1PW91. The center-to-center distance between D and A is 9.98 and 9.92 Å (experimental value, 10.05Å) with corresponding functionals. In the following calculations, the excited states are investigated by the TD-B3LYP functional, using its optimal ground-state structure. In the same way, we employ the TD-MPW1PW91 functional to investigate the excited states, applying its optimized ground-state geometry.

The computed vertical excitation energies, together with the dipole moments, the transition dipole moments, and the oscillator strengths of the excited singlet states of the system, are listed in Table 1. For the DBA system, the first six lowest singlet excited states have been calculated. Although some experimental spectra are available for this DBA system, most of them were obtained in solvents such as tetrahydrofuran (THF), dichloromethane (DCM), and acetonitrile (ACN).[19] In this section, we report the in vacuo absorption feature of the DBA system and make a comparison with experimental results.

As shown in Table 1, our results indicate that two kinds of functionals give almost the same energy order and the same transition feature for the low-lying states of DBA. The highest occupied molecular orbital (HOMO) and the lowest unoccupied molecular orbital (LUMO) of the ground state at the B3LYP/6-31G* level are shown in Figure 1. The calculated results

**TABLE 1: Vertical Excitation Energies of Low-Lying Excited States of DBA in the Gas Phase**

| | state | transition | orbital assignment[a] | $E$/eV[b] | $m_{0i}$/D[c] | $\mu$/D[d] | $f$ | $\Delta q$[e] |
|---|---|---|---|---|---|---|---|---|
| TD-B3LYP/6-31+G* | $S_1$ | HOMO → LUMO | $\pi \rightarrow \pi_d^*$ | 3.36 | 2.23 | 29.63 | 0.064 | 0.62 |
| | $S_2$ | HOMO-1 → LUMO | $\pi \rightarrow \pi_d^*$ | 4.46 | 0.03 | 29.83 | 0.000 | 0.62 |
| | $S_3$ | HOMO → LUMO+2 | $\pi \rightarrow \pi^*$ | 4.78 | 2.94 | 5.17 | 0.156 | 0.11 |
| | $S_4$ | HOMO → LUMO+1 | $\pi \rightarrow \pi_d^*$ | 4.90 | 0.25 | 10.25 | 0.001 | 0.21 |
| | $S_5$ | HOMO-2 → LUMO | $\pi_d \rightarrow \pi_d^*$ | 5.28 | 6.01 | 16.42 | 0.723 | 0.34 |
| | $S_6$ | HOMO → LUMO+3 | $\pi \rightarrow \pi_d^*$ | 5.28 | 0.07 | 8.77 | 0.000 | 0.16 |
| TD-MPW1PW91/6-31+G* | $S_1$ | HOMO → LUMO | $\pi \rightarrow \pi_d^*$ | 3.65 | 2.31 | 29.38 | 0.074 | 0.61 |
| | $S_2$ | HOMO-1 → LUMO | $\pi \rightarrow \pi_d^*$ | 4.82 | 0.02 | 18.74 | 0.000 | 0.39 |
| | $S_3$ | HOMO → LUMO+2 | $\pi \rightarrow \pi^*$ | 4.90 | 2.95 | 11.84 | 0.162 | 0.25 |
| | $S_4$ | HOMO → LUMO+1 | $\pi \rightarrow \pi_d^*$ | 5.10 | 0.23 | 12.70 | 0.000 | 0.26 |
| | $S_5$ | HOMO-2 → LUMO | $\pi_d \rightarrow \pi_d^*$ | 5.42 | 6.00 | 5.75 | 0.740 | 0.12 |
| | $S_6$ | HOMO → LUMO+4 | $\pi \rightarrow \pi^*$ | 5.50 | 1.16 | 2.04 | 0.028 | 0.04 |

[a] $\pi$, $\pi^*$, $\pi_d$, and $\pi_d^*$ refer to the bonding and antibonding $\pi$ orbitals on the catechol moiety and the bonding and antibonding $\pi$ orbitals on the dicyanoethylene group, respectively. [b] $E$ is the relative energy of the excited state with ground-state $S_0$ being taken as zero. [c] $m_{0i}$ is the transition dipole moment between $S_0$ and the $S_i$. [d] The dipole moment in debye. [e] Amount of transferred charge calculated at two functionals in combination with the 6-31+G* basis set.

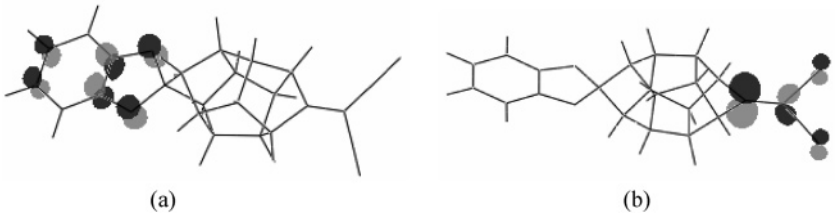


**Figure 1.** HOMO (a) and LUMO (b) of the ground state of the DBA.

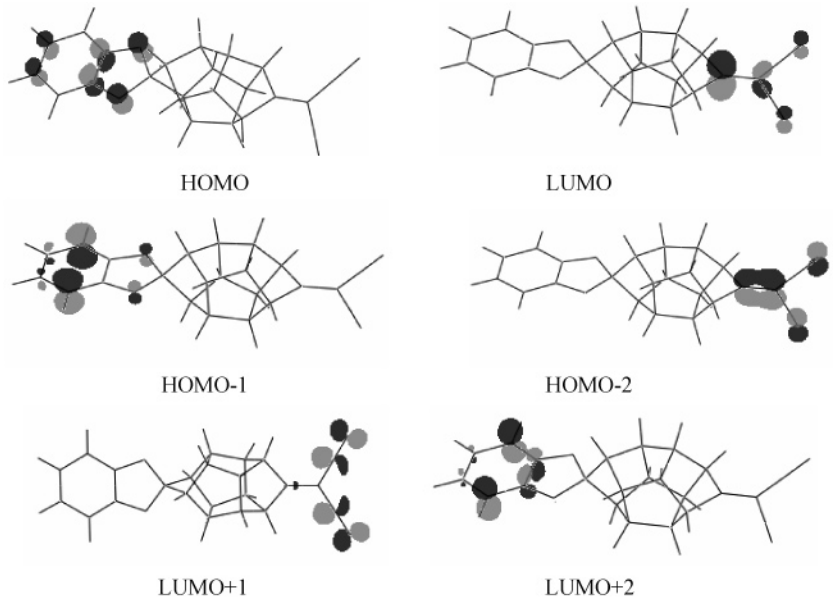


**Figure 2.** Frontier orbitals involved in the low-lying transitions of the DBA.

indicate that the excitation from $S_0$ to $S_1$ is the HOMO → LUMO transition (see Figure 2). HOMO is a $\pi$-type orbital located on the donor, but LUMO is a $\pi^*$-type orbital contributed from the acceptor. Therefore, $S_1$ is a CT state with the characteristic of the $\pi \rightarrow \pi^*$ transition. Similarly, $S_2$, $S_4$, and $S_6$ are also CT states from the TD-B3LYP calculations. However, $S_6$ is a LE state when applying the TD-MPW1PW91 calculation (see Table 1). The dipole moment for state $S_1$ is beyond 29 D through the finite field technique with both functionals. A large change of dipole moment indicates a charge separation in this state. Since TDDFT calculation cannot give directly the charge distribution of the excited state, we adopt an approximate estimation for the amount of transferred charge through the calculated dipole moment and ET distance. For the $S_1$ state, the amount of transferred charge is estimated to be about 0.62 at the TD-B3LYP/6-31+G* level and 0.61 at the TD-MPW1PW91/6-31+G* level. The corresponding excitation energy is ~3.5 eV (see Table 1). The calculated oscillator strength of $S_1$ is not neglectably small; hence we assess that the CT state can be produced through direct photoexcitation. The oscillator strength of the $S_2$ state is almost zero. This implies that the transition $S_0 \rightarrow S_2$ is forbidden.

The two excited states, $S_3$ and $S_5$, possess the largest transition dipole moments and oscillator strengths among the six excited states. LUMO+2 is a $\pi^*$-type orbital localized on the donor but HOMO-2 is a $\pi^*$-type orbital on the acceptor. This implies $S_3$ and $S_5$ are LE states located on the donor and the acceptor, respectively. The amounts of transferred charges for these two states are very small. Our calculations show that LUMO+1 and LUMO+2 are nearly degenerate in energy.

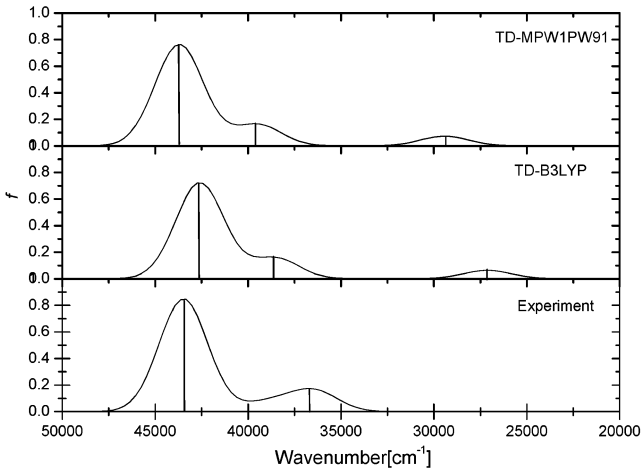


**Figure 3.** Calculated absorption spectra for the DBA using TD-B3LYP results and TD-MPW1PW91 results with the 6-31+G* basis set. The oscillator strength (line) is given as the height of the peak. The lowest panel is from experimental data (see Figures 1−3b of ref 17).

A comparison of the theoretical calculation with the experimental spectrum[19] shows that $S_3$ is responsible for the 280 nm absorption of the $\pi\pi^*$ transition on the catechol moiety, whereas $S_5$ corresponds to the 230 nm of the $\pi\pi^*$ transition on dicyanoethylene. Moreover, the results from the calculations in vacuo show that $S_5$ is the most intense absorption. This coincides with the experimental observation.

From the calculated results, we find there are other spin-allowed $\pi\pi^*$ transitions (see Figure 2), but their oscillator strengths are very small and hence invisible. For example, $S_2$, a CT state, corresponds to the HOMO-1 → LUMO transition, and the corresponding oscillator strength is almost zero and is therefore hidden under the other more intense $\pi\pi^*$ absorptions. To quantify this, the simulated absorption spectra with different functionals are obtained by broadening the theoretical line spectra with Gaussian functions, i.e.,

$$I(\tilde{\nu}) \approx \sum_i f_i \exp\left[-\frac{1}{2}\left(\frac{\tilde{\nu}-\tilde{\nu}_i}{\sigma}\right)^2\right] \qquad (7)$$

where $\sigma = 1300$ cm$^{-1}$ is the width of the Gaussians centered at peak number $i$ with wavenumber $\tilde{\nu}_i$ and oscillator strength $f_i$. The simulated results are given in Figure 3. This procedure roughly accounts for the finite experimental resolution, vibrational and rotational broadening, finite lifetime, and nonvertical transition effects. The bottom panel in Figure 3 is a sketch map based on experimental data.[17] The strongest band is the 230 nm (5.39 eV or 43 478 cm$^{-1}$) absorption of dicyanoethylene, and the second peak at 280 nm (4.43 eV or 35 714 cm$^{-1}$) is from the catechol. As for the middle panel of Figure 3 (based on the result from B3LYP), we assign the intense low-energy peak at 4.78 eV (38 574 cm$^{-1}$) to the HOMO → LUMO+2 transition (see Table 1). We guess this corresponds to the experimentally observed maximum absorption at 280 nm from the LE of the donor. The most intense high-energy peak at about 5.28 eV (42 610 cm$^{-1}$, see Table 1) is assigned to the HOMO-2 → LUMO transition, which corresponds to the 230 nm LE of the acceptor in experiment. The MPW1PW91 functional gives the similar feature of simulated spectra (see the upper panel in Figure 3). However, both B3LYP and MPW1PW91 functuionals predict a small new peak at about 28 000 cm$^{-1}$ that was not found in experiment. A possible reason is their very small oscillator strength.

**3.2. Gas-Phase Absorption of Isolated D, A, B, and DB.** To confirm if the absorption at 280 nm is responsible for a LE state resulting from the $\pi-\pi^*$ transition on catechol moiety or not, we focus on the spectroscopic properties of isolated species and the compound DB in this section. Here DB is composed of the catechol moiety connected with the bridge HCTD. The structures of isolated D, A, B, and compound DB are shown in Chart 2. We use hydrogen atoms to saturate the broken bonds. To keep the integrity of the bridge structure, a carbon atom is added to B and DB (see Chart 2). Of course, these changes of structure will affect the spectroscopic properties, but such influences are expected to be trivial. The optimized geometries for the ground states in vacuo are obtained at the B3LYP/6-31G* and MPW1PW91/6-31G* levels. All the calculated results are collected in Table 2.

As shown in Table 2, the TD-B3LYP calculation for species D gives a dipole-allowed $S_0 \rightarrow S_1$ transition with a vertical excitation energy of 4.90 eV (253 nm). This excited state is characterized as a $\pi \rightarrow \pi^*$ transition, from HOMO to LUMO. The oscillator strength of $S_1$, 0.054, is the largest one among those calculated six excited singlet states (only two are listed in Table 2). Similar results are obtained at the TD-MPW1PW91 level. The absorption band maximum for B is predicted at ∼180 nm. In addition, the band maximum of group A is calculated at about 220 nm (5.60 eV by TD-MPW1PW91 and 5.70 eV by TD-B3LYP), and it arises from the transition HOMO → LUMO. All of these results imply the impossibility that the absorption peak at 280 nm of DBA in experiment arises from the local excitations on A or B. From the transition energies 4.73 (262 nm) (TD-B3LYP) and 4.83 eV (257 nm) (TD-MPW1PW91) of DB, we notice that the $S_1$ state is probably a LE state on the catechol moiety, because DB and D possess almost the same absorption peak. For this reason, we make a predication that the absorption at 280 nm of DBA in experiment is from the LE transition on the donor. In addition, state $S_1$ of the isolated acceptor at about 220 nm can be assigned to the LE on the dicyanoethylene moiety of DBA in experimental observation.[17]

We make a comprehensive view of the excited states discussed in sections 3.1 and 3.2. All the excited states of DBA have nothing to do with the bridge (see Figure 2). In other words, the electron is not transferred via the bridge. After the formation of excited D*BA through photoexcitation, there are two possible pathways to the decay of D*BA: one is to return directly to the ground state, and the other is to form a CT state, $D^+BA^-$. The ET process seems independent of B in any case and it takes place directly from D to A via a tunneling process. This implies the weak coupling between the donor (or acceptor) and the bridge. Therefore, we tentatively conclude that the ET of DBA proceeds via a superexchange mechanism. Although a more quantitative description for the ET mechanism is needed to calculate the value of electronic coupling between the donor and the acceptor, the intuitionistic picture of ET given above is valuable as a rough evaluation.

**3.3. Absorption in Solution.** Considering that the steady-state absorption spectrum of DBA was detected in different solvents, namely, THF, DCM, and CAN[19] (the corresponding dielectric constants are 7.58, 8.93, and 36.64, respectively), we use the continuous medium theory to perform the calculation of the solvent effect. Transition energies of the low-lying excited states of DBA in these three solvents are computed with the PCM[48−50] solvation model in combination with TDDFT (B3LYP and MPW1PW91), using 6-31G*, cc-pVDZ, 6-31+G*, and 6-31++G(d,p) basis sets. To obtain a sufficiently large pool of

**CHART 2**

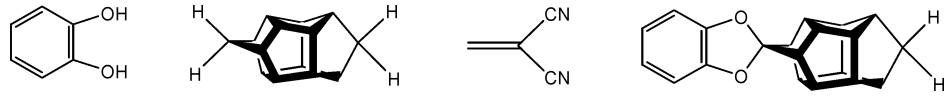


D B A DB

**TABLE 2: Transition Energies of Low-Lying Excited States of Different Species in Vacuo**

| | | | TD-B3LTP/6-31+G* | | | TD-MPW1PW91/6-31+G* | | |
|---|---|---|---|---|---|---|---|---|
| species | state | transition | $E$/eV[a] | $m_{0i}$/D[b] | $f$ | $E$/eV | $m_{0i}$/D | $f$ |
| D | $S_1$ | HOMO → LUMO | 4.90 | 1.71 | 0.054 | 5.00 | 1.72 | 0.056 |
| | $S_2$ | HOMO → LUMO+1 | 4.93 | 0.12 | 0.000 | 5.15 | 0.10 | 0.000 |
| B | $S_1$ | HOMO → LUMO | 6.75 | 0.00 | 0.000 | 6.98 | 0.00 | 0.000 |
| | $S_2$ | HOMO-2 → LUMO | 7.04 | 0.00 | 0.000 | 7.26 | 0.00 | 0.000 |
| A | $S_1$ | HOMO → LUMO | 5.60 | 3.50 | 0.260 | 5.70 | 3.54 | 0.270 |
| | $S_2$ | HOMO-1 → LUMO | 5.65 | 0.00 | 0.000 | 5.79 | 0.00 | 0.000 |
| DB | $S_1$ | HOMO → LUMO | 4.73 | 2.63 | 0.124 | 4.83 | 2.63 | 0.127 |
| | $S_2$ | HOMO → LUMO+1 | 4.89 | 0.24 | 0.001 | 5.12 | 0.23 | 0.001 |

[a] Relative energy of the excited state with ground-state $S_0$ being taken as zero. [b] $m_{0i}$ is the transition dipole moment between $S_0$ and the $S_i$.

**TABLE 3: Vertical Excitation Energies, $E$, Transition Dipole Moments, $m_{0i}$, and Oscillator Strengths, $f$, of the DBA System, Using the TD-DFT/B3LYP Method**

| basis set | | 6-31G* | | cc-pVDZ | | 6-31+G* | | | 6-31++G** | |
|---|---|---|---|---|---|---|---|---|---|---|
| solvent | state | $E$/eV[a] | $f$ ($m_{0i}$/D[b]) | $E$/eV | $f$ ($m_{0i}$/D) | $E$/eV | $f$ ($m_{0i}$/D) | $\Delta E$ [c]/meV | $E$/eV | $f$ ($m_{0i}$/D) |
| THF | $S_1$ | 3.26 | 0.080 (2.55) | 3.31 | 0.082 (2.55) | 3.26 | 0.084 (2.61) | −97.9 | 3.26 | 0.084 (2.60) |
| | $S_2$ | 4.41 | 0.000 (0.05) | 4.47 | 0.000 (0.04) | 4.40 | 0.000 (0.04) | −66.7 | 4.40 | 0.000 (0.04) |
| | $S_3$ | 4.92 | 0.211 (3.37) | 4.85 | 0.205 (3.34) | 4.74 | 0.203 (3.36) | −43.3 | 4.72 | 0.201 (3.35) |
| | $S_4$ | 5.03 | 0.000 (0.02) | 5.13 | 0.000 (0.03) | 4.91 | 0.000 (0.05) | 13.8 | 4.90 | 0.001 (0.28) |
| | $S_5$ | 5.27 | 0.780 (6.25) | 5.26 | 0.789 (6.29) | 5.11 | 0.001 (0.26) | −176.8 | 4.94 | 0.001 (0.26) |
| | $S_6$ | 5.45 | 0.041 (1.41) | 5.38 | 0.042 (1.44) | 5.18 | 0.826 (6.48) | −96.9 | 5.18 | 0.827 (6.48) |
| | $S_7$ | 5.53 | 0.003 (0.36) | 5.51 | 0.003 (0.36) | 5.31 | 0.044 (1.48) | | 5.22 | 0.002 (0.29) |
| | $S_8$ | 5.58 | 0.003 (0.34) | 5.58 | 0.002 (0.34) | 5.40 | 0.003 (0.37) | | 5.30 | 0.044 (1.48) |
| | $S_9$ | 5.71 | 0.000 (0.07) | 5.71 | 0.000 (0.08) | 5.42 | 0.000 (0.11) | | 5.38 | 0.003 (0.36) |
| | $S_{10}$ | 5.90 | 0.000 (0.10) | 5.93 | 0.001 (0.28) | 5.47 | 0.002 (0.34) | | 5.46 | 0.002 (0.34) |
| DCM | $S_1$ | 3.27 | 0.081 (2.55) | 3.31 | 0.083 (2.56) | 3.27 | 0.085 (2.62) | −90.2 | 3.27 | 0.085 (2.61) |
| | $S_2$ | 4.42 | 0.000 (0.04) | 4.48 | 0.000 (0.04) | 4.40 | 0.000 (0.03) | −58.2 | 4.41 | 0.000 (0.04) |
| | $S_3$ | 4.92 | 0.213 (3.38) | 4.85 | 0.206 (3.35) | 4.74 | 0.204 (3.37) | −44.4 | 4.72 | 0.202 (3.36) |
| | $S_4$ | 5.03 | 0.000 (0.02) | 5.12 | 0.000 (0.03) | 4.91 | 0.000 (0.05) | 11.6 | 4.90 | 0.001 (0.25) |
| | $S_5$ | 5.26 | 0.783 (6.26) | 5.26 | 0.787 (6.28) | 5.12 | 0.001 (0.26) | −172.5 | 4.94 | 0.002 (0.29) |
| | $S_6$ | 5.45 | 0.042 (1.42) | 5.37 | 0.043 (1.45) | 5.18 | 0.828 (6.49) | −99.7 | 5.18 | 0.831 (6.50) |
| | $S_7$ | 5.52 | 0.003 (0.36) | 5.50 | 0.003 (0.37) | 5.31 | 0.045 (1.50) | | 5.23 | 0.002 (0.29) |
| | $S_8$ | 5.57 | 0.003 (0.35) | 5.57 | 0.002 (0.34) | 5.39 | 0.003 (0.37) | | 5.30 | 0.045 (1.49) |
| | $S_9$ | 5.71 | 0.000 (0.08) | 5.70 | 0.000 (0.08) | 5.42 | 0.000 (0.09) | | 5.37 | 0.003 (0.37) |
| | $S_{10}$ | 5.90 | 0.000 (0.03) | 5.92 | 0.003 (0.37) | 5.46 | 0.002 (0.34) | | 5.45 | 0.002 (0.34) |
| ACN | $S_1$ | 3.28 | 0.079 (2.52) | 3.32 | 0.081 (2.53) | 3.28 | 0.084 (2.59) | −77.3 | 3.28 | 0.083 (2.58) |
| | $S_2$ | 4.44 | 0.000 (0.04) | 4.49 | 0.000 (0.04) | 4.42 | 0.000 (0.03) | −42.8 | 4.42 | 0.000 (0.03) |
| | $S_3$ | 4.92 | 0.205 (3.31) | 4.85 | 0.198 (3.29) | 4.74 | 0.197 (3.31) | −42.3 | 4.72 | 0.195 (3.30) |
| | $S_4$ | 5.00 | 0.000 (0.02) | 5.10 | 0.000 (0.03) | 4.88 | 0.000 (0.04) | −21.0 | 4.88 | 0.000 (0.11) |
| | $S_5$ | 5.28 | 0.772 (6.20) | 5.28 | 0.776 (6.23) | 5.14 | 0.001 (0.25) | −143.0 | 4.96 | 0.003 (0.37) |
| | $S_6$ | 5.45 | 0.040 (1.38) | 5.37 | 0.040 (1.40) | 5.20 | 0.816 (6.43) | −83.2 | 5.20 | 0.819 (6.44) |
| | $S_7$ | 5.48 | 0.002 (0.33) | 5.45 | 0.003 (0.36) | 5.31 | 0.042 (1.45) | | 5.25 | 0.001 (0.27) |
| | $S_8$ | 5.53 | 0.002 (0.34) | 5.53 | 0.002 (0.33) | 5.33 | 0.003 (0.36) | | 5.30 | 0.042 (1.44) |
| | $S_9$ | 5.67 | 0.000 (0.08) | 5.66 | 0.000 (0.08) | 5.41 | 0.002 (0.33) | | 5.32 | 0.003 (0.36) |
| | $S_{10}$ | 5.86 | 0.002 (0.32) | 5.88 | 0.006 (0.51) | 5.44 | 0.000 (0.07) | | 5.41 | 0.002 (0.33) |

[a] Relative energy of the excited state with ground-state $S_0$ being taken as zero. [b] $m_{0i}$ is the transition dipole moment between $S_0$ and $S_i$. [c] $\Delta E$ is the solvation shift, which is the difference of transition energy in solution (this table) minus that in vacuo given in Table 1.

excited states for the relevant excitations, in Tables 3 and 4 we report the first 10 vertical excitation energies, the oscillator strengths, and transition dipole moments in solution.

As listed in Table 3, in THF, DCM, and ACN, the calculations at TD-B3LYP/6-31+G* and TD-B3LYP/6-31++G(d,p) levels indicate that $S_1$ is contributed mainly from the HOMO → LUMO transition, $S_2$ mainly from HOMO-1 → LUMO, $S_4$ from HOMO → LUMO+1 excitation, and $S_5$ from HOMO → LUMO+3 transition. Similar to the situation shown in Figure 2, HOMO-1 and HOMO are $\pi$-type orbitals located on the donor moiety, whereas LUMO, LUMO+1, and LUMO+3 are $\pi$*-type orbitals on the acceptor A in solvents. Thus, $S_1$, $S_2$, $S_4$, and $S_5$ are CT states with an electron transferring from the $\pi$ orbital of the donor to the $\pi$* orbital of the acceptor. Their orbital assignment is $\pi \rightarrow \pi_d$* ($\pi$ and $\pi$* refer to the bonding and antibonding $\pi$ orbitals located on the catechol moiety, respectively; $\pi_d$ and $\pi_d$* represent the bonding and antibonding $\pi$ on the dicyanoethylene group, see Table 1). The state $S_3$ exhibits the behavior of $\pi \rightarrow \pi$* transition from HOMO to LUMO+2 and is of the feature of LE on the donor. The same analysis shows the $S_6$ state (HOMO-2 → LUMO) is also a LE state but on the acceptor, assigned as the $\pi_d \rightarrow \pi_d$* transition. For excited states $S_7$, $S_8$, $S_9$, and $S_{10}$, the calculated results indicate their excitations are disorder in these three solvents at both TD-B3LYP/6-31+G* and TD-B3LYP/6-31++G(d,p) levels. Such as $S_7$ is mainly from the HOMO → LUMO+4 transition

**TABLE 4: Vertical Excitation Energies, *E*, Transition Dipole Moments, $m_{0i}$, and Oscillator Strengths, *f*, of the DBA System, Using the TD-DFT/ MPW1PW91 Method**

| basis set | | 6-31G* | | cc-pVDZ | | 6-31+G* | | | 6-31++G** | |
|---|---|---|---|---|---|---|---|---|---|---|
| solvent | state | *E*/eV | $f(m_{0i}$/D) | *E*/eV[a] | $f(m_{0i}$/D[b]) | *E*/eV | $f(m_{0i}$/D) | Δ*E*/meV | *E*/eV | $f(m_{0i}$/D) |
| THF | $S_1$ | 3.55 | 0.091 (2.60) | 3.58 | 0.092 (2.60) | 3.54 | 0.095 (2.65) | −106.4 | 3.54 | 0.095 (2.65) |
| | $S_2$ | 4.74 | 0.000 (0.04) | 4.79 | 0.000 (0.03) | 4.72 | 0.000 (0.03) | −103.0 | 4.72 | 0.000 (0.03) |
| | $S_3$ | 5.02 | 0.211 (3.33) | 4.94 | 0.204 (3.30) | 4.84 | 0.203 (3.32) | −55.0 | 4.83 | 0.201 (3.31) |
| | $S_4$ | 5.38 | 0.824 (6.36) | 5.36 | 0.820 (6.35) | 5.27 | 0.000 (0.12) | 170.7 | 5.10 | 0.002 (0.34) |
| | $S_5$ | 5.39 | 0.000 (0.02) | 5.48 | 0.000 (0.03) | 5.30 | 0.860 (6.54) | −118.7 | 5.28 | 0.000 (0.03) |
| | $S_6$ | 5.56 | 0.042 (1.41) | 5.48 | 0.043 (1.43) | 5.33 | 0.001 (0.19) | −169.7 | 5.30 | 0.861 (6.55) |
| | $S_7$ | 5.63 | 0.003 (0.35) | 5.61 | 0.003 (0.35) | 5.42 | 0.044 (1.47) | | 5.45 | 0.001 (0.25) |
| | $S_8$ | 5.74 | 0.003 (0.36) | 5.73 | 0.003 (0.35) | 5.53 | 0.003 (0.36) | | 5.51 | 0.003 (0.35) |
| | $S_9$ | 5.91 | 0.000 (0.09) | 5.91 | 0.000 (0.10) | 5.64 | 0.003 (0.35) | | 5.63 | 0.003 (0.35) |
| | $S_{10}$ | 6.05 | 0.000 (0.07) | 6.11 | 0.011 (0.69) | 5.67 | 0.000 (0.05) | | 5.64 | 0.000 (0.00) |
| DCM | $S_1$ | 3.55 | 0.092 (2.61) | 3.59 | 0.093 (2.61) | 3.55 | 0.096 (2.79) | −98.3 | 3.55 | 0.096 (2.66) |
| | $S_2$ | 4.75 | 0.000 (0.04) | 4.80 | 0.000 (0.03) | 4.73 | 0.000 (0.03) | −94.2 | 4.73 | 0.000 (0.03) |
| | $S_3$ | 5.01 | 0.212 (3.34) | 4.94 | 0.205 (3.31) | 4.84 | 0.204 (3.33) | −56.0 | 4.82 | 0.202 (3.32) |
| | $S_4$ | 5.37 | 0.827 (6.37) | 5.36 | 0.823 (6.36) | 5.27 | 0.000 (0.10) | 170.9 | 5.11 | 0.002 (0.34) |
| | $S_5$ | 5.39 | 0.000 (0.02) | 5.48 | 0.000 (0.03) | 5.30 | 0.863 (6.56) | −121.2 | 5.27 | 0.000 (0.02) |
| | $S_6$ | 5.56 | 0.043 (1.42) | 5.48 | 0.043 (1.44) | 5.33 | 0.000 (0.19) | −165.3 | 5.29 | 0.865 (6.56) |
| | $S_7$ | 5.62 | 0.003 (0.35) | 5.60 | 0.003 (0.36) | 5.42 | 0.045 (1.48) | | 5.45 | 0.001 (0.25) |
| | $S_8$ | 5.73 | 0.003 (0.36) | 5.72 | 0.003 (0.35) | 5.52 | 0.003 (0.36) | | 5.50 | 0.003 (0.35) |
| | $S_9$ | 5.91 | 0.000 (0.10) | 5.90 | 0.000 (0.11) | 5.63 | 0.003 (0.35) | | 5.62 | 0.003 (0.35) |
| | $S_{10}$ | 6.04 | 0.000 (0.07) | 6.10 | 0.012 (0.71) | 5.67 | 0.000 (0.04) | | 5.65 | 0.000 (0.00) |
| ACN | $S_1$ | 3.57 | 0.090 (2.58) | 3.60 | 0.091 (2.58) | 3.56 | 0.094 (2.59) | −84.9 | 3.56 | 0.094 (2.63) |
| | $S_2$ | 4.77 | 0.000 (0.03) | 4.81 | 0.000 (0.03) | 4.75 | 0.000 (0.03) | −78.4 | 4.75 | 0.000 (0.02) |
| | $S_3$ | 5.02 | 0.204 (3.27) | 4.94 | 0.198 (3.25) | 4.84 | 0.196 (3.31) | −53.2 | 4.83 | 0.195 (3.27) |
| | $S_4$ | 5.36 | 0.000 (0.02) | 5.38 | 0.813 (6.31) | 5.25 | 0.000 (0.04) | 143.9 | 5.13 | 0.002 (0.34) |
| | $S_5$ | 5.39 | 0.817 (6.32) | 5.45 | 0.000 (0.03) | 5.31 | 0.852 (0.25) | −103.0 | 5.24 | 0.000 (0.03) |
| | $S_6$ | 5.56 | 0.040 (1.39) | 5.48 | 0.041 (1.40) | 5.35 | 0.001 (6.43) | −143.1 | 5.31 | 0.854 (6.51) |
| | $S_7$ | 5.57 | 0.002 (0.32) | 5.55 | 0.003 (0.35) | 5.42 | 0.042 (1.45) | | 5.41 | 0.042 (1.43) |
| | $S_8$ | 5.68 | 0.003 (0.35) | 5.68 | 0.002 (0.34) | 5.46 | 0.003 (0.36) | | 5.44 | 0.003 (0.35) |
| | $S_9$ | 5.87 | 0.000 (0.10) | 5.86 | 0.000 (0.11) | 5.58 | 0.002 (0.33) | | 5.49 | 0.001 (0.24) |
| | $S_{10}$ | 6.02 | 0.000 (0.06) | 6.05 | 0.012 (0.72) | 5.69 | 0.000 (0.07) | | 5.58 | 0.002 (0.33) |

[a] Relative energy of the excited state with ground-state $S_0$ being taken as zero. [b] $m_{0i}$ is the transition dipole moment between $S_0$ and $S_i$.

at the TD-B3LYP/6-31+G* level in ACN, at the TD-B3LYP/6-31++G(d,p) level in DCM the same transition is $S_8$. It is well-known that the TD-DFT method will give reliable results for low-lying states,[20,21,23,39,40] but the reason of the disorder in higher excitation states remains unclear. In addition, in the present work, we focus on the LE states $S_3$ and $S_6$, hence the higher excited states are less important to our discussion. The values of transition dipole moment and oscillator strength (Table 3) show that the transitions from ground-state $S_0$ to $S_3$ and $S_6$ are comparatively strong. For $S_3$, the excitation energies in THF, DCM, and ACN are about 4.74 eV at different levels. Therefore, we specify $S_3$ to the 280 nm (4.43 eV) $\pi\pi^*$ transition of the catechol moiety in experimental observation. The strongest absorption band of state $S_6$ (the excitation energies of $S_6$ in THF, DCM, and ACN are around 5.20 eV at different levels, see Table 3) corresponds to a LE absorption peak at 230 nm (5.39 eV) observed in experiment. Considering the uncertainty in experimental determinations of the band-origin peak and the error in the computations (0.1−0.2 eV), we feel our theoretical calculations are in good agreement with the experimental measurements. In addition, in solvents, the results using TD-MPW1PW91/6-31+G* and TD-MPW1PW91/6-31++G(d,p) are similar to those discussed above. However, it must be emphasized that the LE transition at 230 nm in experimental results is $S_5$ at the TD-MPW1PW91/6-31+G* level. Furthermore, we find the results calculated with the 6-31++G(d,p) basis set are nearly identical with those calculated with the 6-31+G* basis set. Hence the 6-31+G* basis set is adequate for our case and we apply it in the following section.

We consider the solvent effects on the absorption spectra with an increase of the solvent polarity. The calculated results at different levels are given in Table 3. The solvation shift is defined as the difference between the excited energy of state $S_i$ in solvent and that in vacuo. In solvents, the state $S_5$ is responsible for the strong band at 230 nm when we perform the TD-MPW1PW91/6-31+G* calculation. This coincides with the prediction in vacuo. However, the band at 230 nm results from state $S_6$ when TD-B3LYP/6-31+G* is adopted. Thus, at this level, the value of the solvation shift should be the difference between the excited energy of the $S_6$ state in solvent and that of $S_5$ in vacuo. Red shifts of absorption spectra are predicted in our work. As shown in Table 3, the magnitudes of the red shift are very small. The red shift is 97.9 meV in THF, 90.2 meV in DCM, and 77.3 meV in ACN for the $S_1$ state of DBA at the TD-B3LYP/6-31+G* level. There is a slight decrease for the absolute value of the solvation shift with the increase of solvent polarity. Similar features can be found for the rest of the states except for $S_4$, whose change of solvation shift is not well-regulated with the increase of solvent polarity. Further, we find the TD-MPW1PW91/6-31+G* results are similar to the TD-B3LYP/6-31+G* results. That is, the solvation shift slightly decreases with the increase of solvent polarity.

The absorption spectra in three solvents are shown in Figure 4 by using eq 7. Obviously, the absorption profiles at the TD-B3LYP/6-31+G* level are almost the same in different solvents. This predication is in agreement with the experimental observation.[19] From the oscillator strength calculation, we see that the dominant transitions are $S_0 \rightarrow S_3$ and $S_0 \rightarrow S_6$, which correspond to the vertical LE of the donor and that of the acceptor, respectively. For the former, the excitation energies in different solvents are ∼4.74 eV (38 252 $cm^{-1}$), but for the later, the results are about 5.18 eV (41 803 $cm^{-1}$). Therefore, the $\pi\pi^*$ absorption peak at 4.74 eV can be ascribed definitely to the low-lying energy band of the catechol moiety, and the $\pi\pi^*$ band at about 5.18 eV is attributed to the LE of the dicyanoethylene group. Similar to the situation in vacuo, our results display a

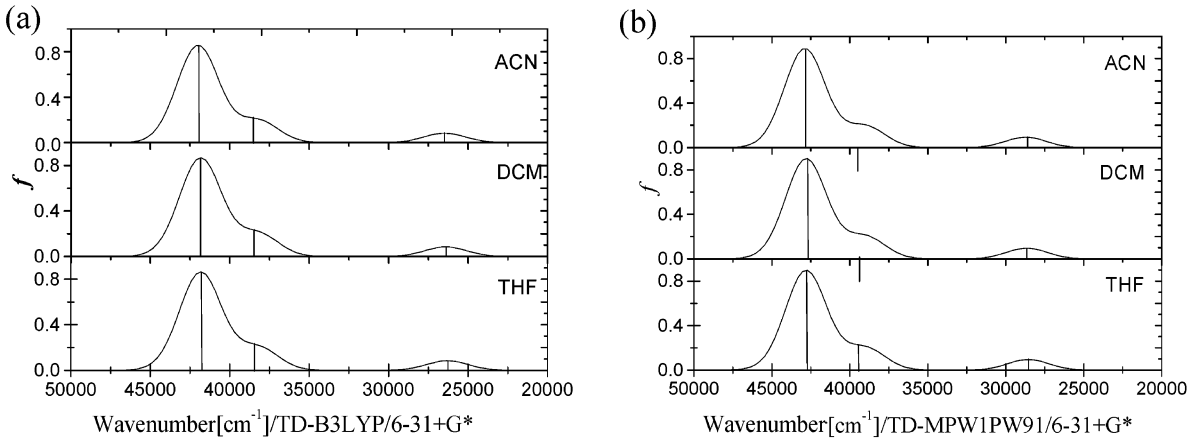


**Figure 4.** Calculated absorption spectra for DBA in solvents at the levels of TD-B3LYP/6-31+G* (a) and TD-MPW1PW91/6-31+G* (b). Oscillator strengths (*f*) of the computed transitions (lines) are given. Please see 3b of Figure 1 in ref 24 for comparison.

third peak with a small oscillator strength, which corresponds to the $S_0 \rightarrow S_1$ excitation. We assign this to a CT transition (see Figure 4). Therefore, we predict that the CT state can also be produced through direct photoexcitation, besides the decay from the higher LE states. However, the experimental observation shows that the CT band arises uniquely from the decay from the LE of the catechol moiety.[19] This indicates a gap between our theoretical predication and the experimental assessment.

As listed in Table 4, when the TD-MPW1PW91/6-31+G* is applied in solvents, some expected results are obtained. Comparing with the TD-B3LYP/6-31+G* results, TD-MPW1PW91/6-31+G* always gives higher excitation energies. Moreover, TD-MPW1PW91 calculations predict a LE state $S_5$ on the dicyanoethylene group, but in the case of TD-B3LYP, this LE state shifts to $S_6$. When TD-B3LYP and TD-MPW1PW91 combining with 6-31G* and cc-pVDZ basis sets are applied to the DBA system in solvents, the results are also similar to those in vacuo. It is notable that the transition order has a large change in these calculations. For example, in the case of TD-B3LYP, $S_5$ is the HOMO-2 $\rightarrow$ LUMO transition, but in the case of TD-MPW1PW91 the HOMO-2 $\rightarrow$ LUMO excitation is $S_4$ except for the 6-31G* result in ACN (see Table 4). It is further found that the TD-MPW1PW91 excitation energies are always higher than those with TD-B3LYP, independent of the basis sets. The excitation energies can be improved by increasing the basis sets size from 6-31G* to cc-pVDZ and to 6-31+G* for both finctionals, which denotes the exact positions of the absorption peak depend sensitively on the quality of the basis sets. In particular, diffuse functions are required for larger molecules such as the present DBA system. However, it seems that no remarkable improvement can be made by expanding the size of basis sets beyond 6-31++G(d,p).

On the basis of the discussions above, it is found the addition of the diffuse functions leads to a change of 0.15 eV of average excitation energy, while both functionals B3LYP and MPW1PW91 give the average differences of about 0.22 eV. In addition, two functionals in combination with the same basis set give very similar energy orders and transition features in solvent.

**3.4. Electronic Coupling Matrix Element.** In this section, we pay attention to the ET dynamics through the electronic coupling matrix element $H_{ij}$, and make a comparison with the experiment result.[19] We select the TD-B3LYP and TD-MPW1PW91 functionals in combination with the 6-31+G* basis set to perform the calculations of the $H_{ij}$ in vacuo. The values of $H_{ij}$ for the transition between the excited states and the ground state, calculated using eq 6, are listed in Table 5. We find that both functionals give the almost identical change trend of $H_{ij}$ (see Table 5). It is obvious that the values of $H_{03}$ and $H_{05}$ are much larger than those of $H_{01}$, $H_{02}$, $H_{04}$, and $H_{06}$ for the TD-B3LYP results. According to Fermi's Golden rule, the ET rate constant is proportional to the square of $H_{ij}$. Hence the ET rate from the ground state to $S_3$ and $S_5$ states can be predicted much faster than that to $S_1$, $S_2$, $S_4$, and $S_6$. On the basis of theoretical calculations in section 3.1, we know that the states $S_3$ and $S_5$ are LE states, and $S_1$, $S_2$, $S_4$, and $S_6$ are CT states. Therefore, it seems that the ET rate from the ground state to LE states is much faster than that to CT states. Furthermore, for the TD-MPW1PW91 results, $S_6$ is also a LE state (see Table 1). So we find the values of $H_{03}$, $H_{05}$, and $H_{06}$ are very large in this level (Table 5). Thus, these results enable us to make a prediction that the LE state is produced first and its population amount will be much larger than that of the CT state in the primary photoexcitation process. This means that the main absorption in the plot of the absorption spectra is due to LE, rather than the CT absorption (Figure 4). In experiment, the detected spectra were always due to LE transitions located on the catechol moiety (at 280 nm) and on the dicyanoethylene group (at 230 nm).[17,19] Therefore, our results show a good agreement with the experimental observations (see Figures 1−3b of ref 17).

**TABLE 5: Electronic Coupling Matrix Element between the Ground State and the Excited Ones (in meV)**

| | TD-B3LYP/6-31+G* | | | TD-MPW1PW91/6-31+G* | | |
|---|---|---|---|---|---|---|
| | $\mu$/D | $m_{0i}$ /D | $H_{0j}$ | $\mu$/D | $m_{0i}$ /D[b] | $H_{0j}$ |
| $S_0 \rightarrow S_1$ | 29.63 | 2.23 | 315.5 | 29.38 | 2.31 | 362.4 |
| $S_0 \rightarrow S_2$ | 29.83 | 0.03 | 5.7 | 18.74 | 0.02 | 7.9 |
| $S_0 \rightarrow S_3$ | 5.17 | 2.94 | 2330.7 | 11.84 | 2.95 | 1829.4 |
| $S_0 \rightarrow S_4$ | 10.25 | 0.25 | 324.7 | 12.70 | 0.23 | 191.5 |
| $S_0 \rightarrow S_5$ | 16.42 | 6.01 | 2037.4 | 5.75 | 6.00 | 2701.4 |
| $S_0 \rightarrow S_6$ | 8.77 | 0.07 | 163.2 | 2.04 | 1.16 | 1248.6 |

## 4. Conclusion

In this work, we report the theoretical absorption spectra and properties of excited states of the DBA model system concerned, by means of the TD-DFT (B3LYP and MPW1PW91) method together with 6-31G*, cc-pVDZ, 6-31+G*, and 6-31++G(d,p) basis sets. The predictions with two functionals combined with a series of basis sets are found valuable, and the results from these calculations are consistent. According to the theoretical results, we draw a conclusion that the two most intense absorptions are of the characteristics of $\pi-\pi^*$ and LE transition.

Our study shows the absorption peak of DBA is almost independent of the solvent polarity. All of the calculated results are in good agreement with the experimental observations. In addition, it seems that the CT state is possibly produced through direct photoexcitations, although only LE absorptions were observed in experiments. Through the analysis of molecular orbitals and the features of excited states, we suggest that the intramolecular ET possibly takes place via the superexchange mechanism. Electronic coupling matrix element calculations using GMH theory indicate that the main absorption of the model system is attributed to the LE absorption.

**Acknowledgment.** This work is supported by the National Natural Science Foundation of China (No. 20473054).

## References and Notes

(1) Jortner, J. *J. Chem. Phys*. **1976**, *64*, 4860−4867.
(2) Armitage, B. *Chem. Rev*. **1998**, *98*, 1171−1200.
(3) Zerza, G.; Scharber, M. C.; Brabec, C. J.; Sariciftci, N. S.; Gómez, R.; Segura, J. L.; Martín, N.; Srdanov, V. I. *J. Phys. Chem. A*. **2000**, *104*, 8315−8322.
(4) Pourtois, G.; Beljonne, D.; Cornil, J.; Ratner, M. A.; Brédas, J. L. *J. Am. Chem. Soc*. **2002**, *124*, 4436−4447.
(5) (a) La Chair, J. J. *Angew. Chem., Int. Ed. Engl*. **1999**, *38*, 3045−3047. (b) La Chair, J. J. *Angew. Chem., Int. Ed. Engl*. **1998**, *37*, 325−329.
(6) Singh, A. K.; Darshi, M.; Kanvah, S. *J. Phys. Chem. A* **2000**, *104*, 464−471.
(7) Metzger, R. M. *J. Mater. Chem*. **2000**, *10*, 55−62.
(8) La Chair, J. J. *J. Am. Chem. Soc*. **1997**, *119*, 7676−7684.
(9) Chen, J.; Reed, M. A.; Rawlett, A. M.; Tour, J. M. *Science*. **1999**, *286*, 1550−1552.
(10) Cao, L.; Chen, H.; Wang, M.; Sun, J. *J. Phys. Chem. B* **2002**, *106*, 8971−8975.
(11) Prasanna de Silva, A.; Nimal Gunaratne, H. Q.; Gunnlaugsson, T.; Huxley, A. J. M.; McCoy, C. P.; Rademacher, J. T.; Rice, T. E. *Chem. Rev*. **1997**, *97*, 1515−1566.
(12) Yu, C. J.; Chong, Y.; Kayyem, J. F.; Gozin, M. *J. Org. Chem*. **1999**, *64*, 2070−2079.
(13) Lewis, F. D.; Wu, T. F.; Zhang, Y. F.; Letsinger, R. L.; Greenfield, S. R.; Wasielewski, M. R. *Science*. **1997**, *277*, 673−676.
(14) Gust, D.; Moore, T. A.; Moore, A. L. *Acc. Chem. Res*. **1993**, *26*, 198−205.
(15) Wasielewski, M. R. *Chem. Rev*. **1992**, *92*, 435−461.
(16) Balzani, V.; Juris, A.; Venturi, M.; Campagna, S.; Serroni, S. *Chem. Rev*. **1996**, *96*, 759−934.
(17) Chiou, N. R.; Chow, T. J.; Chen, C. Y.; Hsu, M. A.; Chen, H. C. *Tetrahedron Lett*. **2001**, *42*, 29−31.
(18) Chow, T. J.; Hon, Y. S.; Chen, C. Y.; Huang, M. S. *Tetrahedron Lett*. **1999**, *40*, 7799−7801.
(19) Chow, T. J.; Chiu, N. R.; Chen, H. C.; Chen, C. Y.; Yu, W. S.; Cheng, Y. M.; Cheng, C. C.; Chang, C. P.; Chou, P. T. *Tetrahedron* **2003**, *59*, 5719−5730.
(20) Wiberg, K. B.; Olibeira, A. E.; Trucks, G. *J. Phys. Chem. A* **2002**, *106*, 4192−4199.
(21) Gross, E. K. U.; Ullrich, C. A.; Gossmann, U. J. In *Density Functional Theory*; Gross E. K. U., Dreizler, R. M., Eds.; NATA ASI Series; Plenum: New York, 1994; p 149.
(22) Hirata, S.; Ivanov, S.; Grabowski, I.; Bartlett, R. J. *J. Chem. Phys.* **2002**, *116*, 6468−6481.
(23) Bauernschmitt R.; Ahlrichs, R. *Chem. Phys. Lett*. **1996**, *256*, 454−464.
(24) Handy, N. C.; Tozer, D. J. *J. Comput. Chem.* **1999**, *20*, 106−113.
(25) Zyubin, A. S.; Mebel, A. M. *J. Chem. Phys.* **2003**, *119*, 6581−6587.
(26) (a) Yi, H.-B.; Duan, X.-H.; KimK. S. *J. Chem. Phys.* **2003**, *119*, 8854−8862. (b) Naleway, C. A.; Curtiss, L. A.; Miller, J. R. *J. Phys. Chem*. **1991**, *95*, 8434−8437. (c) Duan, X.-H.; Li, Z.-R.; Li, X.-Y.; Li, L.-M. *J. Chem. Phys.* **2004**, *120*, 10025−10032.
(27) Kelley, S. O.; Barton, J. K. *Science* **1999**, *283*, 375−381.
(28) Tolbert, L. M. *Acc. Chem. Res.* **1992**, *25*, 561−568.
(29) Arrhenius, T. S.; Blanchard-Desce, M.; Dvolaitzky, M.; Lehn, J. M.; Malthete, J. *Proc. Natl. Acad. Sci. U.S.A.* **1986**, *83*, 5355−5359.
(30) Winkler, J. R.; Gray, H. B. *Chem. Rev*. **1992**, *92*, 369−379.
(31) Moser, C. C.; Keske, J. M.; Warncke, K.; Farid, R. S.; Dutton, P. L. *Nature* **1992**, *355*, 796−802.
(32) Newton, M. D. *Chem. Rev*. **1991**, *91*, 767−792.
(33) Mikkelsen, K. V.; Ratner, M. A. *Chem. Rev.* **1987**, *87*, 113−153.
(34) Kestner, N. R.; Logan, J.; Jortner, J. *J. Phys. Chem*. **1974**, *78*, 2148−2166.
(35) Efrima, S.; Bixon, M. *Chem. Phys*. **1976**, *13*, 447−460.
(36) Jortner, J. *J. Chem. Phys*. **1976**, *64*, 4860−4867.
(37) Cave, R. J.; Newton, M. D. *Chem. Phys. Lett*. **1996**, *249*, 15−19.
(38) Frisch, M. J.; Trucks, G. W.; Schlegel, H. B.; et al. *Gaussian 03*; Gaussian, Inc.: Pittsburgh, PA, 2003.
(39) Jamorski, C.; Casida, M. E.; Salahub, D. R. *J. Chem. Phys.* **1996**, *104*, 5134−5147.
(40) Hirata, S.; Head-Gordon, M. *Chem. Phys. Lett*. **1999**, *314*, 291−299.
(41) Jödicke, J. C.; Foresman, J. B.; Thilgen, C.; Lthi, H.-P. *J. Chem. Phys.* **2002**, *116*, 8761−8771.
(42) Jödicke, J. C.; Lthi, H. P. *J. Chem. Phys.* **2002**, *117*, 4146−4156.
(43) Jödicke, J. C.; Lthi, H. P. *J. Chem. Phys.* **2002**, *117*, 4157−4167.
(44) Zhan, C.-G.; Dixon, D. A.; Sabri, M. I.; Kim, M.-S.; Spencer, P. S. *J. Am. Chem. Soc.* **2002**, *124*, 2744−2752.
(45) Runge, E.; Gross, E. K. U. *Phys. Rev. Lett.* **1984**, *52*, 997−1000.
(46) Onsager, L. *J. Am. Chem. Soc*. **1936**, *58*, 1486-1493.
(47) Wong, M. W.; Frisch, M. J.; Wiberg, K. B. *J. Am. Chem. Soc.* **1991**, *113*, 4776−4782.
(48) Wong, M. W.; Wiberg, K. B.; Frisch, M. J. *J. Am. Chem. Soc.* **1992**, *114*, 523−529.
(49) Zhan, C.-G.; Bentley, J.; Chipman, D. M. *J. Chem. Phys.* **1998**, *108*, 177−192.
(50) Cossi, M.; Rega, N.; Scalmani, G.; Barone, V. *J. Chem. Phys.* **2001**, *114*, 5691−5701.